2017 13th IEEE International Conference on Control & Automation (ICCA)
July 3-6, 2017. Ohrid, Macedonia

Aircraft Spiral Dive Attractors Due To Actuator Saturation*

Po-Chun Chan[1], Sevket F. Catpinar[2], Bor-Chin Chang[3] *IEEE Member*,
Harry Kwatny[4] *IEEE Fellow*, Christine M. Belcastro[5] *IEEE Senior Member*

***Abstract*— Under extreme adverse flight conditions, such as extreme turbulence, the aircraft controller may send a large control command attempting to counter the resulting forces and moments on the vehicle. In doing so, it may cause the actuator to saturate and operate at its extreme limit. The sustained actuator saturation may cause a loss of control authority and force the aircraft to move towards an undesired dangerous attractor instead of the desired flight trim. In the case study of F/A-18, two of these types of undesired spiral dive attractors have been identified. Once an aircraft is seized by the attractor, it would lose altitude and crash if no proper action is taken in time. A two-mode switching scheme has been incorporated into the LOC (loss-of-control) recovery controller to successfully prevent sustained actuator saturation, eliminate the threat of the spiral dive attractors, and enhance the LOC recovery control.**

I. Introduction

Feedback control has played a significant role in almost every aspect of modern civilization since James Watt's flyball governor invention for steam engines that ignited the Industrial Revolution at the turn of the 19th Century. About a hundred years later, shortly after the Wright Brothers invented the airplane, Wilber Wright visioned that "the age of flying" will have arrived when "this one feature (the ability to balance and steer)" has been worked out [1]. The age of flying certainly has arrived, and the implementation of feedback control theory has greatly improved the ability to balance and steer and enhanced the safety, quality, and performance of the flight. However, a feedback control system occasionally may do more harm than help if it is not properly designed to deal with the issue of sustained actuator saturation, which is caused by the wind-up phenomena [2] [3] [4] of the control input commands. The sustained actuator saturation will not only cause a loss of control authority, it will also force the aircraft to be drawn to a dangerous undesired flight attractor - in the case study of this paper it is a spiral dive flight with -82.9° flight path going down. The spiral dive attractor is a serious safety threat, which certainly needs to be addressed.

*This work was supported in part by Army Research Laboratory under contract W911NF-15-2-0042.

[1]Department of Mechanical Engineering, Drexel University, Philadelphia, PA 19104, U.S.A. pc366@drexel.edu

[2]Department of Mechanical Engineering, Drexel University, Philadelphia, PA 19104, U.S.A. sfc38@drexel.edu

[3]Department of Mechanical Engineering, Drexel University, Philadelphia, PA 19104, U.S.A. bchang@coe.drexel.edu

[4]Department of Mechanical Engineering, Drexel University, Philadelphia, PA 19104, U.S.A. hkwatny@coe.drexel.edu

[5]NASA Langley Research Center, MS161, Hampton, VA 23681, U.S.A. Christine.M.Belcastro@nasa.gov

One way to avoid sustained actuator saturation is to keep the control input commands below the saturation limits all the time, but it may not be practical to do so since the amount of control input required is event dependent. Under extreme conditions, larger control effort usually is required. In aircraft LOC (loss-of-control) recovery control [5], [6], almost every case is extreme since aircraft LOC is an abnormal flight condition that includes stall, unusual attitude, large pitch and roll motion, and lateral/longitudinal oscillations, etc., which may pose a safety threat to the aircraft if no immediate action is taken to address it. Therefore, the LOC recovery control system needs to be designed not only to recover aircraft from the LOC conditions, but also to avoid sustained actuator saturation. Note that the actuator saturation would not cause problem if it only occurs for a short period of time. The issue is the wind-up phenomena that may lead to the sustained actuator saturation.

The focus of this paper is not to propose a new anti-windup approach or to do a literature survey comparing the existing anti-windup papers for the best solution. Instead, we will firstly concentrate on exploring how a sustained actuator saturation would cause aircraft to lose its stability and crash. Then we will look for a feasible solution accordingly. After browsing hundreds of existing anti-windup papers in the literature we were unable to find one that employed a fidelity full nonlinear aircraft simulation model to demonstrate its effectiveness in dealing with this critical flight safety issue. Although some in the literature did consider nonlinear aircraft flight dynamics, they were either incomplete consisting of only part of the dynamics or they just represented the dynamics at a fixed trim only.

The rest of the paper is organized as follows. Section II will provide a brief description of the full untrimmed nonlinear F/A-18 flight dynamics simulation model with actuator limits and dynamics constraints. A short review of the aircraft trim, equilibrium, linearized model, and the LOC prevention/recovery controller will also be included in this section. In Section III, we will describe how sustained actuator saturation can lead the aircraft to one of the twin spiral dive flight attractors. In Section IV, a two-mode switching scheme is designed to integrate the Zaccarian and Teel's anti-windup filter structure [7] with the LOC recovery controller to prevent sustained actuator saturation and recover the aircraft back to a desired flight trim. The simulation results with the full untrimmed nonlinear F/A-18 model in Section V will demonstrate the capability of the proposed approach, and Section VI is the conclusion.

978-1-5386-2679-5/17/$31.00 ©2017 IEEE

II. PRELIMINARIES

A. The F/A-18 Aircraft Flight Dynamics Model

The F/A-18 Aircraft Flight Dynamics Model employed in this paper is the same as the one we used for aircraft loss-of-control recovery study in [8]. This full untrimmed 12-state nonlinear Simulink model was assembled based on the works of Chakraborty et. al [9] [10] and Buttrill et. al[11]. The 12-state nonlinear F/A-18 Aircraft Flight Dynamics Model and its associated state variables and control inputs are briefly described in the following.

$$\begin{aligned} &\dot{x}(t) = f(x(t), u(t)) \\ &x = \left[\begin{array}{cccccccccccc} V & \beta & \alpha & p & q & r & \phi & \theta & \psi & pN & pE & h \end{array}\right]^T \\ &u = \left[\begin{array}{cccc} \delta_a & \delta_r & \delta_e & \delta_T \end{array}\right]^T \end{aligned} \tag{1}$$

The 12 state variables are V: total speed (ft/s), β: side slip (rad), α: angle of attack (rad), p: roll rate (rad/s), q: pitch rate (rad/s), r: yaw rate (rad/s), ϕ: roll angle (rad), θ: pitch angle (rad), ψ: yaw angle (rad), pN: position North (ft), pE: position East (ft), h: altitude (ft). The 4 control inputs are δ_a: aileron (rad), δ_r:rudder (rad), δ_e:elevator (rad), δ_T:Thrust (lbf) [12]. Note that the unit for all angles or angular rates in actual computations will be in radians or rad/s. However, for the ease of comprehension by human, the angles or angular rates will be displayed in degrees or deg/s. The equations of motion inside Eq.(1) are given [8]. The actuator dynamics constraints of saturation and rate are given as follows:

$$\begin{gathered} -25^\circ < \delta_a < 25^\circ,\ -30^\circ < \delta_r < 30^\circ,\ -24^\circ < \delta_e < 10.5^\circ \\ 0\text{lbf} < \delta_T < 20,000\text{lbf},\ -100^\circ/s < \dot{\delta}_a < 100^\circ/s, \\ -61^\circ/s < \dot{\delta}_r < 61^\circ/s,\ -40^\circ/s < \dot{\delta}_e < 40^\circ/s \end{gathered} \tag{2}$$

and the actuator dynamics of δ_a, δ_r, δ_e, and δ_T, are given by $48/(s+48)$, $40/(s+40)$, $30/(s+30)$, and $30/(s+30)$, respectively.

B. Trim, Equilibrium, and Linearization

The aircraft flight dynamics equations are nonlinear, flight condition-dependent, and can be highly coupled. A common practice of flight control system design is to choose a flight trim associated with a desired flight condition, and obtain a linear 12-state model to represent the flight dynamics at and around the trim. Owing to the symmetrical structure of the aircraft under most of the normal flight conditions, the linearized model can be further simplified by decoupling the model into two sets of state equations including the longitudinal and the lateral state equations.

In aircraft flight dynamics, an equilibrium is a flight condition at which the following eight state variables: V, β, α, p, q, r, ϕ, and θ can remain as constant at steady state. A trim is a flight equilibrium we would like the aircraft to fly. For example, a straight level flight with 10° angle of attack is a trim, which is called Trim A for later reference in the paper,

$$\begin{aligned} x_{trimA} = &\left[\begin{array}{cccccccc} 435.9\text{ft/s} & 0^\circ & 10^\circ & 0^\circ/s & 0^\circ/s \\ 0^\circ/s & 0^\circ & 10^\circ & *^\circ & *\text{ft} & *\text{ft} & *\text{ft} \end{array}\right]^T \\ u_{trimA} = &\left[\begin{array}{cccc} 0^\circ & 0^\circ & -1.26^\circ & 5470.5\text{lbf} \end{array}\right] \end{aligned} \tag{3}$$

Note that the values of the yaw angle (ψ), the two position (pN and pE), and the altitude (h) are left open since they are dependent on the other 8 state variables and not required to be constant at a steady state. In addition, not every equilibrium can serve as a trim. For example, the dangerous spiral dive attractors described in Section I are equilibriums but neither is qualified to serve as a trim. To study the flight dynamics at and around $Trim\ A$, we will obtain the linearized state-space model at this trim via Jocobian approach and decouple it into the following longitudinal and lateral dynamics equations.

$$\begin{aligned} &\dot{\bar{x}}_{Lg}(t) = A_{Lg}\bar{x}_{Lg}(t) + B_{Lg}\bar{u}_{Lg}(t) \\ &\bar{x}_{Lg} = \left[\begin{array}{cccc} \bar{V} & \bar{\alpha} & \bar{q} & \bar{\theta} \end{array}\right]^T, \quad \bar{u}_{Lg} = \left[\begin{array}{cc} \bar{\delta}_e & \bar{\delta}_T \end{array}\right]^T \\ &A_{Lg} = \left[\begin{array}{cccc} -0.0239 & -28.3172 & 0 & -32.2 \\ -0.0003 & -0.3621 & 1 & 0 \\ 0 & -2.2115 & -0.2532 & 0 \\ 0 & 0 & 1 & 0 \end{array}\right], \\ &B_{Lg} = \left[\begin{array}{cc} -3.8114 & 0.001 \\ -0.0515 & 0 \\ -2.8791 & 0 \\ 0 & 0 \end{array}\right] \end{aligned} \tag{4}$$

$$\begin{aligned} &\dot{\bar{x}}_{La}(t) = A_{La}\bar{x}_{La}(t) + B_{La}\bar{u}_{La}(t) \\ &\bar{x}_{La} = \left[\begin{array}{cccc} \bar{\beta} & \bar{p} & \bar{r} & \bar{\phi} \end{array}\right]^T, \quad u_{La} = \left[\begin{array}{cc} \bar{\delta}_a & \bar{\delta}_r \end{array}\right]^T \\ &A_{La} = \left[\begin{array}{cccc} -0.0347 & 0.1736 & -0.9848 & 0.0727 \\ -8.543 & -0.8883 & 0.8762 & 0 \\ 0.886 & 0.0399 & -0.1895 & 0 \\ 0 & 1 & 0.1763 & 0 \end{array}\right] \\ &B_{La} = \left[\begin{array}{cc} -0.0149 & 0.0207 \\ 8.3321 & 0.9541 \\ -0.042 & -0.6277 \\ 0 & 0 \end{array}\right] \end{aligned} \tag{5}$$

The longitudinal eigenvalues are located at $-0.3094 \pm j1.499$, $-0.0101 \pm j0.1008$ and the lateral eigenvalues are at $-0.2873 \pm j1.4530$, -0.4888 , -0.0518. The trim is stable although it is oscillatory and lightly damped.

C. Schematic Diagram for LOC Recovery Simulation

To show how the LOC recovery simulations are conducted, we will start from the simulation schematic diagram shown in Fig. 1. The block on the right is the aircraft flight dynamics model, which is described in Section IIA. The output $\hat{u}$ of the Actuator Saturation Limits block normally is the same as the input u (or u_a) except when the input is beyond the limits specified in Eq.(2). The output y, which includes the state variable vector x and all measurable variables, and the input $\hat{u}$ are assumed available for feedback. The Selection Switch on the right of the controllers in general can be controlled by an automatic switching logic or by the pilot based on flight mode changes or special situations. In addition to the pilot manual control, two feedback controllers K_R and K_{RA} are shown on the left side of the Selection Switch. Both K_R and K_{RA} are LOC recovery controllers designed w.r.t. $Trim\ A$ - the only difference is that K_{RA} is equipped with an anti-windup scheme. The structure and design of the

controller K_A will be given in Section IID, and the details of K_{RA} will be discussed in Section IV. To demonstrate

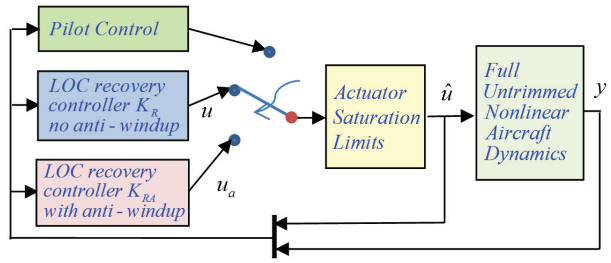

Fig. 1: Schematic diagram for LOC recovery simulation.

an LOC recovery, first of all an LOC scenario would need to be created in the simulation. As conducted in [8] and [9], we would employ the following two initial state vectors, denoted by x_0^G, x_0^H, to represent two LOC scenarios created by previous disturbances or erroneous control actions.

$$x_0^G = \begin{bmatrix} 436\text{ft/s} & 10^\circ & 40^\circ & -20^\circ/s & 0^\circ/s & -10^\circ/s \\ 0^\circ & 10^\circ & 0^\circ & 0\text{ft} & 0\text{ft} & 45000\text{ft} \end{bmatrix}^T$$
$$x_0^H = \begin{bmatrix} 500\text{ft/s} & -20^\circ & 15^\circ & 40^\circ/s & 5^\circ/s & 15^\circ/s \\ 20^\circ & 5^\circ & 0^\circ & 0\text{ft} & 0\text{ft} & 45000\text{ft} \end{bmatrix}^T \quad (6)$$

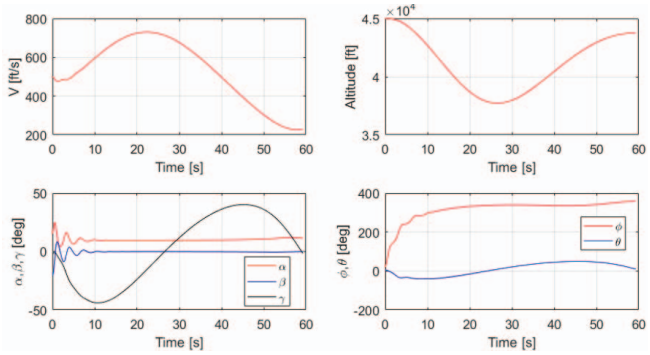

Fig. 2: The response due to x_0^H with no controller.

Note that the disturbances represented by the above two initial states are hostile LOC precursors, who virtually are foretelling the coming of very violent flight conditions. The response of the aircraft due to x_0^H, is shown in Fig. 2. The aircraft is trimmed at Trim A but with no recovery controller. It can be seen from the graphs that within 3 seconds the aircraft has rolled to the right by more than 180° and pitched down to -35°, which certainly is a very difficult LOC situation. Then the aircraft continued its wild ride: it rolls to about 360° position completing one full 360° roll excursion, and pitches up and down between -35° and $+50^\circ$, with a light damping for a long period of time. The flight path angle γ, the speed V and the altitude h also exhibit the up and down excursions.

D. LOC Recovery Controller K_R

The structure of the K_R controller is shown in Fig. 3, in which the two H_2 (or LQR) optimal controllers [13] [14], F_{Lg} and F_{La} are specifically designed for the aircraft to operate in the vicinity of $Trim\ A$. Based on the longitudinal and lateral state equation in Eq.(4) and Eq.(5) respectively, the optimal longitudinal and lateral state feedback controllers are found as,

$$\bar{u}_{Lg}(t) = F_{Lg}\bar{x}_{Lg}$$
$$F_{Lg} = \begin{bmatrix} -0.0028 & -0.2725 & 0.1370 & 0.3315 \\ -0.0326 & -0.7685 & 0.9373 & 1.4266 \end{bmatrix} \quad (7)$$

$$\bar{u}_{La}(t) = F_{La}\bar{x}_{La}$$
$$F_{La} = \begin{bmatrix} 0.8739 & -0.8937 & -0.3573 & -0.3094 \\ -1.8130 & -0.7223 & 2.6598 & -0.1995 \end{bmatrix} \quad (8)$$

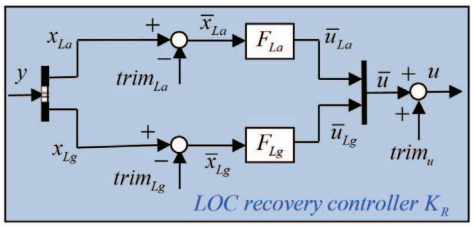

Fig. 3: Recovery Controller K_R designed w.r.t. Trim A.

The switch from the manual control to the K_R controller has changed the longitudinal eigenvalues from $-0.3094 \pm j1.4799$, $-0.0101 \pm j0.1008$, which are the eigenvalues of A_{Lg}, to $-0.3344 \pm j1.4927$, $-0.1702 \pm j0.1126$, which are the eigenvalues of $A_{Lg} + B_{Lg}F_{Lg}$. Note that the damping ratio has changed from $\varsigma = 0.1$ to $\varsigma = 0.834$ and the natural frequency from $\omega_n = 0.101\text{rad/s}$ to 0.204rad/s. Meanwhile, the lateral eigenvalues have changed from $-0.2873 \pm j1.453$, -0.4888, -0.0518, which are the eigenvalues of A_{La}, to $-0.9858 \pm j0.9773$, -8.6583, -0.3258, which are the eigenvalues of $A_{La} + B_{La}F_{La}$. Note that the increases of both damping ratio and natural frequency for both longitudinal and lateral dynamics have enhanced the stability and increased the rate of convergence to the desired $Trim\ A$.

The controller K_R is capable of bringing the LOC aircraft back to the safe flight condition, Trim A, if the controller is engaged soon enough. For the case of LOC scenario caused by the disturbance represented by x_0^H, the window of time to accomplish a successful recovery is between $t = 0s$ and $t = 2.2s$.

III. Spiral Dive Attractors

The time of controller engagement is critical since the LOC condition caused by x_0^H would continue to get worse and become more difficult to control as time goes by. For the case of LOC scenario caused by x_0^H, the controller K_R can accomplish a successful recovery if it engages before $t = 2.2s$. On the other hand, if the controller is engaged at $t = 2.3s$ or later, the controller will need to issue larger control input commands to the actuators attempting to bring the worsening LOC condition into control. But, the aircraft does not have the actuator resources demanded by the controller and hence some actuators have to sustain the saturation values, which is equivalent to jam actuators

at extreme positions. As a result of the sustained actuator saturation, the aircraft would fly towards an undesired spiral dive attractor.

Two undesired spiral dive attractors have been identified. They are described by Eq.(9) and Eq.(10). Both of them are spiral dive flights, one spiraling to the right and the other to the left, with the same $-82.9°$ flight path angle going down. These two equilibriums are called attractors because the aircraft can be easily drawn into one of these two equilibriums if sustained actuator saturation occurs. We have tested the controller K_R with many LOC scenarios caused by the disturbances represented by a variety of initial conditions x_0 and all the failed flights are ended up at one of these two attractors.

$$\begin{aligned} &\textit{Spiral Dive X Attractor}: \\ &x_{diveX} = \left[\ 403.3\text{ft/s} \quad 9.9° \quad 38.9° \quad -50.5°/s \quad -3.2°/s \right. \\ &\quad \left. -40.3°/s \quad -355.4° \quad -51.3° \quad * \quad *\text{ft} \quad *\text{ft} \quad *\text{ft} \ \right]^T \\ &u_{diveX} = \left[\ 25° \quad -17.8° \quad -24° \quad 5469.6\text{lbf} \ \right]^T \end{aligned} \tag{9}$$

$$\begin{aligned} &\textit{Spiral Dive Y Attractor}: \\ &x_{diveY} = \left[\ 403.3\text{ft/s} \quad -9.9° \quad 38.9° \quad 50.5°/s \quad -3.2°/s \right. \\ &\quad \left. 40.3°/s \quad 355.4° \quad -51.3° \quad * \quad *\text{ft} \quad *\text{ft} \quad *\text{ft} \ \right]^T \\ &u_{diveY} = \left[\ -25° \quad 17.8° \quad -24° \quad 5469.6\text{lbf} \ \right]^T \end{aligned} \tag{10}$$

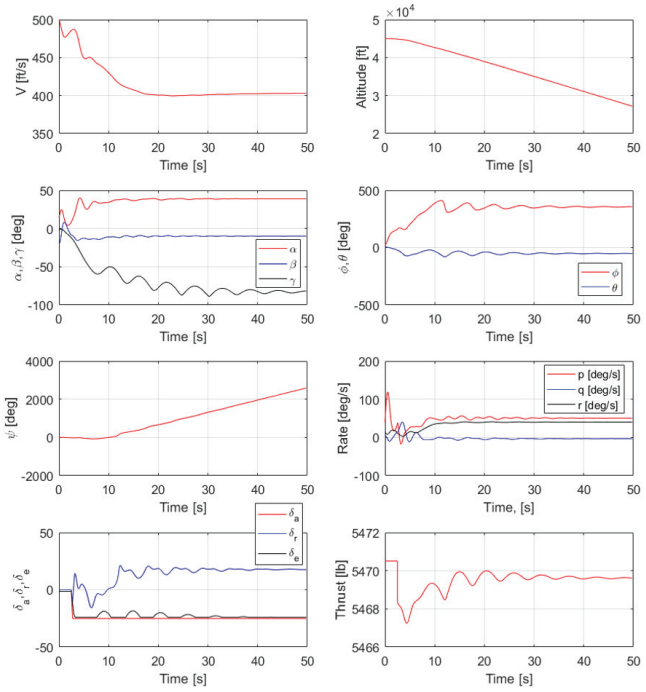

Fig. 4: The response due to x_0^H with the LOC recovery controller K_R engaged at $t = 2.5s$.

Fig. 4 recorded the response of the system due to the initial state x_0^H with the LOC recovery controller K_R engaged at $t = 2.5s$. Apparently the controller K_R was unable to rescue the aircraft from the LOC condition; instead, the aircraft was heading towards one of the spiral dive attractors due to the aileron and elevator sustained saturation. It can be

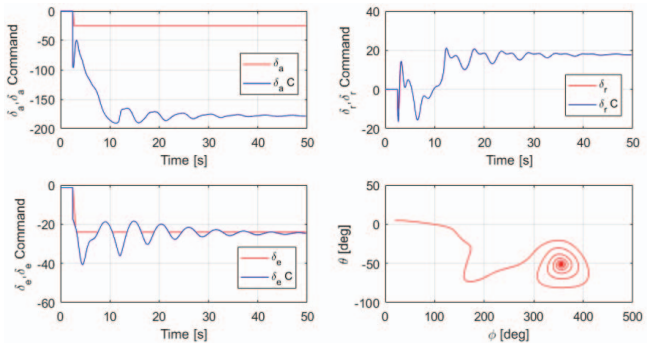

Fig. 5: Saturation of δ_a and δ_e, and θ-ϕ plot.

seen from the simulation graphs in Fig. 4 and Fig. 5 when the controller engaged at $t = 2.5s$ the aircraft had been rolling to the right by $180°$ and continuing. Attempting to stop and reverse the roll, the controller sent a strong aileron command with $\delta_a = -100°$. This command was beyond the limit and hence the aileron actuator saturated at its limit $-25°$. The aileron command magnitude continued to grow beyond the saturation limit and eventually increased all the way to about $-180°$, which continued to keep the aileron in the saturation position $-25°$ throughout the simulation. Meanwhile, the pitch rate was on the rise that prompted the elevator command to go down to about $-40°$, which was also beyond the $-24°$ limit. Then it moved up and down several times before eventually settling at $-24°$, the elevator saturation position, shortly after $t = 30s$. By $t = 30s$, all the eight equilibrium state variables and the four actuator variables are already in the vicinity of the *Spiral Dive Y* attractor described in Eq.(10).

For the second scenario in which the disturbance represented by the initial state vector x_0^G described in Eq.(6) was applied, the time window for the same controller K_R to accomplish a successful recovery and bring the aircraft to the desired flight at $Trim\ A$ was found to be between $t = 0s$ and $t = 1.6s$. The controller would fail to rescue the aircraft from the LOC condition if the controller K_R engaged at $t = 1.7s$ or later. The aircraft would roll to the left to about $-355°$ position despite the controller's effort to increase the aileron command to $+180°$, which will guard the aileron actuator from leaving the saturation position at $+25°$. Shortly after this, the elevator actuator also sustained its saturation position $-24°$ and all the state variables and actuators were converging to the undesired *Spiral Dive X* attractor described by Eq.(9).

These two attractors are dangerous. An aircraft with sustained aileron saturation would have no other equilibrium to go to except being drawn to one of the two insidious attractors. Simulations showed that all the failed K_R LOC recovery feedback control system had ended up going to either of the two undesired spiral dive attractors. Once an aircraft is in either of the spiral dive attractors, the aircraft would spiral down with $-82.9°$ flight path angle and lose altitude at the rate of about 400ft per second, which means the aircraft with $40,000$ ft altitude would crash in less than 100 seconds.

In Section IV, we will seek a solution in controller design to prevent the aircraft from being drawn into any of these dangerous spiral dive attractors.

IV. LOC Recovery Controller K_{RA} with Anti-Windup

The K_R LOC recovery control failure cases in Section III were all initiated by sustained aileron saturations. The windup large aileron command in fact jammed the aileron at the extreme saturation position and hence eliminated all possible safe equilibriums for the aircraft to fly. Some existing actuator anti-windup solutions in [2] [3] [4] and the references therein may be employed to prevent the sustained actuator saturations.

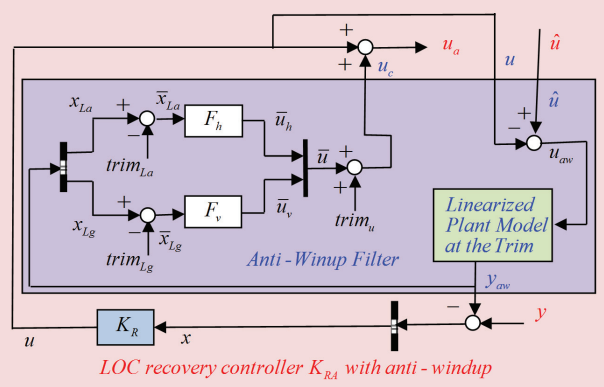

Fig. 6: Schematic diagram for K_{RA}.

The Zaccarian and Teel's anti-windup filter structure [7] is employed to incorporate into the LOC recovery controller to prevent the control input commands from winding up. The schematic diagram of this anti-windup LOC recovery controller K_{RA} is shown in Fig. 6. A simple event-trigger switching mechanism based on the information of $\hat{u}$ and u is employed to select either K_R or K_{RA}, one at a time. The anti-windup filter has two inputs: u and $\hat{u}$, and two outputs: y_{aw} and u_c, and within the filter there are a copy of the plant model and a cloned controller. The plant model is a linearized model of the F/A-18 flight dynamics at $Trim\ A$, and the cloned controller has the same structure as K_R although the controller gain matrices F_v and F_h are not necessarily the same as those in K_R. The difference of u and $\hat{u}$, $u_{aw} = \hat{u} - u$, serves as the input to the plant model copy to generate the output y_{aw}, whose information was lost in the output y due to the actuator saturation. The information of this output y_{aw}, together with the real output y, is fed back to the controller K_R so that the controller will not continue its wrong path of winding up the control input commands blindly. Furthermore, y_{aw} is also fed back to the cloned controller to generate a control input command correction vector u_c to modify the control input command from u to $u_a = u + u_c$. This correction allows the controller to reverse its control input command so that the actuators will not stay at the saturation for too long.

The controller gain matrices F_v and F_h in the anti-windup filter are also constructed based on the H_2 or LQR optimal control theory, but they are chosen to achieve a better anti-windup so that the actuators will not sustain saturations. The matrices F_v and F_h are computed based on the longitudinal and lateral state equations in Eq.(4) and Eq.(5), respectively, as follows,

$$\bar{u}_v(t) = F_v \bar{x}_{Lg}$$
$$F_v = \begin{bmatrix} -0.0976 & 1.8707 & 2.0196 & 3.8348 \\ -0.0113 & 0.1366 & 0.0450 & 0.0650 \end{bmatrix} \quad (11)$$

and

$$\bar{u}_h(t) = F_h \bar{x}_{La}$$
$$F_h = \begin{bmatrix} -2.3052 & -3.1829 & -0.8218 & -3.0608 \\ -8.0309 & -0.2695 & 10.5400 & 0.2562 \end{bmatrix} \quad (12)$$

V. Two-Mode Switching of the LOC Recovery Controllers K_R and K_{RA}

As described in Section III, both of the two LOC scenarios caused by x_0^G, and x_0^H require the LOC controller K_R to engage early. The K_R recoverable engagement time windows for the LOC scenarios associated with x_0^G, and x_0^H are 1.6s, and 2.2s, respectively. If the controller is engaged late, not only it will fail to rescue the aircraft, the situation may get worse due to the sustained actuator saturation, which can lead the aircraft to an undesired disastrous spiral dive. The recoverable time window provided by the LOC recovery controller K_R alone is too short to be practical.

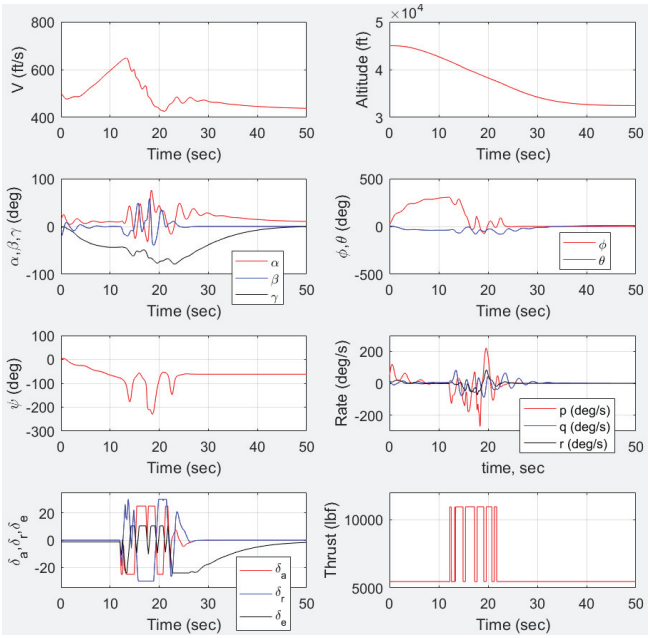

Fig. 7: The response due to x_0^H with the proposed switching mechanism involving LOC recovery controllers K_{RA} and K_R engaged at $t = 12.0s$.

Fortunately, recoverable time window can be significantly improved using the proposed two-mode switching scheme involving both of the LOC recovery controllers K_R and K_{RA}. As demonstrated in Fig. 7 and Fig. 8, the LOC condition due to initial state vector x_0^H can still be successfully recovered

by the late engagement of the two-mode switching LOC control system at $t = 12.0s$.

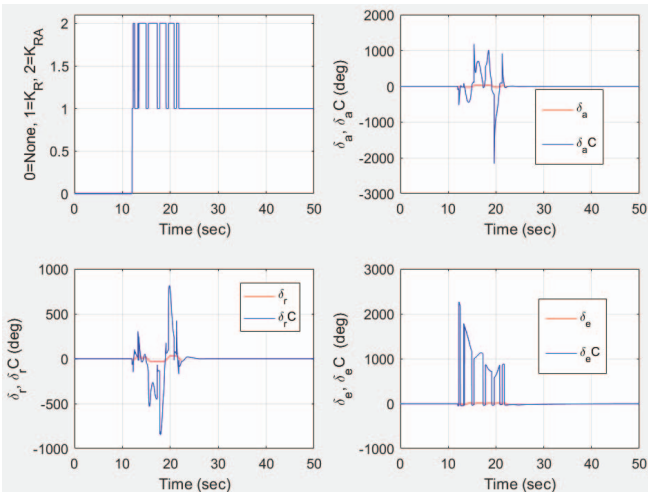

Fig. 8: Two-mode switching between K_{RA} and K_R.

In the upper left graph of Fig. 8, there are three values on the vertical axis: 0, 1, and 2. The values "0" means that no feedback control is applied, "1" represents that the regular LOC recovery controller K_R (with no anti-windup) is turned on, and "2" indicates that the special LOC recovery controller K_{RA} (with anti-windup) has replaced K_R. It can be seen that no feedback controller is engaged before $t = 12.0s$ and K_R is turned on right after $t = 12.0s$ when the control system is engaged. Then the switch jumps back and forth between K_R and K_{RA} several times before it jumps back to K_R at $t = 21.76s$ for the rest of the flight. Fig. 8 also displays the aileron command δ_aC, the rudder command δ_rC, and the elevator command δ_eC as functions of time. The extremely large magnitude of the surface control commands is not a concern since the commands will be clipped off to the saturation values before they can reach and affect the aircraft flight dynamics. The commands are changing and reversing quickly that do not allow the actuators to stay at their saturations for too long to establish an actuator sustained saturation.

Note that in Fig. 7 the three surface control actuators and the thrust control cooperate seamlessly to achieve the LOC recovery control objective although they bounced back and forth between their saturation limits several times before finding a correct path towards the desired flight equilibrium, $Trim\ A$, the straight level flight with 10° angle of attack. It is also interesting to see that the thrust normally operates around 5,467 lbf, but always jumped up to around 10944.56 lbf during the periods when the anti-windup mechanism is on. This discrete jump is caused by the mode change of the system. Overall, it is a hybrid switching control system that switches back and forth between two operational modes: one with the anti-windup mechanism and the other without it.

VI. CONCLUSION

The full 12-state/4-control-input untrimmed nonlinear F/A-18 flight dynamics simulation model has been employed to demonstrate that a flight control system without a reliable anti-windup protection may be susceptible to sustained actuator saturation. The sustained saturation would then lead the aircraft to one of the two hostile spiral dive attractors. These two attractors are identical in every aspect except the spiral orientation. Both are a serious threat since an aircraft with sustained actuator saturation would have no other equilibrium to go to except being drawn to one of the two insidious attractors.

Once an aircraft is in the vicinity of the attractors, it will lose altitude rapidly and a crash is imminent. To eliminate the threat of the spiral dive attractors, we have incorporated an anti-windup filter structure in the design of the LOC recovery control system. The proposed event-trigger switching mechanism, LOC recovery controller, and the anti-windup scheme together have resolved the sustained actuator saturation issue, eliminated the threat of the spiral dive attractors, expanded the region of attraction of the control system, and greatly improved the success rate of LOC recovery control.

REFERENCES

[1] W. Wright. (1901) Some aeronautical experiments. [Online]. Available: http://invention.psychology.msstate.edu/i/Wrights/library/Aeronautical.html

[2] L. Zaccarian and A. R. Teel, *Modern anti-windup synthesis: control augmentation for actuator saturation*. Princeton University Press, 2011.

[3] V. Kapila and K. Grigoriadis, *Actuator Saturation Control*. CRC Press, 2002.

[4] G. Leonov, B. Andrievskii, N. Kuznetsov, and A. Y. Pogromskii, "Aircraft control with anti-windup compensation," *Differential equations*, vol. 48, no. 13, pp. 1700–1720, 2012.

[5] C. M. Belcastro and J. V. Foster, "Aircraft loss-of-control accident analysis," in *Proceedings of the 2010 AIAA Guidance, Navigation, and Control Conference*, Toronto, Canada, Aug. 2010.

[6] C. M. Belcastro, L. Groff, L. Newman, J. V. Foster, D. A. Crider, and D. H. Klyde, "Preliminary analysis of aircraft loss of control accidents: Worst case precursor combinations and temporal sequencing," in *Proceedings of the 2014 AIAA Guidance, Navigation, and Control Conference*, National Harbor, MAryland, Jan. 2014.

[7] L. Zaccarian and A. R. Teel, "A common framework for anti-windup, bumpless transfer and reliable designs," *Automatica*, vol. 38, no. 10, pp. 1735–1744, 2002.

[8] B. Chang, H. Kwatny, E. Ballouz, and D. Hartman, "Aircraft trim recovery from highly nonlinear upset conditions," in *Proceedings of the 2016 AIAA Guidance, Navigation, and Control Conference AIAA2016-0880*, 2016, pp. 1–19.

[9] A. Chakraborty, P. Seiler, and G. J. Balas, "Susceptibility of f/a-18 flight controllers to the falling-leaf mode: Nonlinear analysis," *Journal of guidance, control, and dynamics*, vol. 34, no. 1, pp. 73–85, 2011.

[10] ——, "Susceptibility of f/a-18 flight controllers to the falling-leaf mode: Linear analysis," *Journal of guidance, control, and dynamics*, vol. 34, no. 1, pp. 57–72, 2011.

[11] C. S. Buttrill, P. D. Arbuckle, and K. D. Hoffler, "Simulation model of a twin-tail, high performance airplane," 1992.

[12] B. L. Stevens, F. L. Lewis, and E. N. Johnson, *Aircraft Control and Simulation: Dynamics, Controls Design, and Autonomous Systems*, 2015.

[13] D. J., G. K., K. P., and F. B., "State-space solutions to standard h_2 and h_∞ optimal control problems," *IEEE Transactions on Automatic control*, vol. 33, pp. 831–847, 1989.

[14] K. G. K. Zhou, J. Doyle, *Robust and Optimal Control*. Prentice Hall, 1996.